JACS
JOURNAL OF THE AMERICAN CHEMICAL SOCIETY

pubs.acs.org/JACS

Communication

Transformation Network Culminating in a Heteroleptic $Cd_6L_6L'_2$ Twisted Trigonal Prism

Dawei Zhang, Tanya K. Ronson, Lin Xu,* and Jonathan R. Nitschke*

Cite This: J. Am. Chem. Soc. 2020, 142, 9152–9157

Read Online

ACCESS | Metrics & More | Article Recommendations | Supporting Information

ABSTRACT: Transformations between three-dimensional metallosupramolecular assemblies can enable switching between the different functions of these structures. Here we report a network of such transformations, based upon a subcomponent displacement strategy. The flow through this network is directed by the relative reactivities of different amines, aldehydes, and di(2-pyridyl)ketone. The network provides access to an unprecedented heteroleptic $Cd_6L_6L'_2$ twisted trigonal prism. The principles underpinning this network thus allow for the design of diverse structural transformations, converting one helicate into another, a helicate into a tetrahedron, a tetrahedron into a different tetrahedron, and a tetrahedron into the new trigonal prismatic structure type. The selective conversion from one host to another also enabled the uptake of a desired guest from a mixture of guests.

The development of new stimulus-induced transformations between self-assembled architectures is an important challenge in supramolecular chemistry.[1] Such transformations mimic the structural changes of biological molecules,[2] potentially leading to biomimetic functions, such as catalysts that may be modulated using cofactors, as with enzymes.[3] Differences in guest binding properties between interconvertible container molecules[4] also allow for the design of new functions, such as controllable guest uptake and release,[5] chemical purification,[6] reagent storage,[7] and drug delivery.[8] Although stimuli such as light,[5b,9] pH,[10] temperature,[11] solvent,[12] or concentration[13] can induce cages to respond in useful ways, linking these factors together to generate networks of transformations remains a challenging goal.[1a]

Complex metal–organic structures[14] made using subcomponent self-assembly[15] can transform due to the dynamic nature of both the coordinative (N → metal) and covalent (N=C) bonds that knit these structures together. The displacement of one subcomponent for another thus serves as a general strategy for structural interconversion.[16]

As different amines and aldehydes generate metal imine complexes that are more or less stable, the addition of new amines and aldehydes to existing structures can induce these structures to rearrange in well-defined ways through subcomponent substitution.[16] Electronic effects[17] and steric hindrance[18] can serve as driving forces for rearrangement. The presence of multiple distinct subcomponents may also lead to the formation of new heteroleptic assemblies.[19] The arrangements of the different subcomponents within these heteroleptic assemblies may bring about lower symmetries, helping to enable the binding of complex, low-symmetry substrates.[20]

Here we demonstrate the use of subcomponent displacement as an efficient method for bringing about structural transformations within a network of interconverting assemblies. This study led to the discovery of a new type of heteroleptic trigonal prismatic host having anion binding properties.[21] The transformations within the network also enabled selective guest uptake from solution.

We recently reported the use of the subcomponent di(2-pyridyl)ketone **A**. This ketone imparts improved acid resistance to its imine metal complexes, as compared to 2-formylpyridine, as a result of its free basic pyridyl units at the corners.[22]

Mixture of ketone **A** (6 equiv), triamine **B** (3 equiv), and cadmium trifluoromethanesulfonate (triflate, TfO^-, 2 equiv) produced Cd_2L_3 triple helicate **1a** (Figures 1 and S3–S10). Complex **1a** is the first member of a new family of helicates containing free basic pyridyl units and amine functionalities.

Although numerous attempts to obtain the crystal structure of Cd_2L_3 **1a** were unsuccessful, we were able to obtain the crystal structure of its Fe^{II} analogue **1b**, which was synthesized similarly (Figures S11–S18). As shown in Figure 1a, the two iron(II) centers of **1b**, separated by a distance of 13.9 Å, have the same handedness, generating a structure with D_3 symmetry. Only two of the amines from each residue of **B** condensed with ketone **A**, leading to the formation of C_2-symmetric bis-bidentate ligands. Complex **1b** thus contains six uncoordinated pyridyl units in total around its two vertices. The vertices of **1b** are constrained due to the potential steric clash between these free pyridyl rings and the neighboring phenylene rings (Figure S85a).[22]

The addition of bis-amine **C** (3 equiv) to **1a** led to the formation of new helicate **2**, releasing subcomponent **B** (Figures 1, S19–S26, and S88). Similarly, addition of triamine **F** (3 equiv) to **1a** produced helicate **4** (Figures S35–S42 and

Received: April 7, 2020
Published: May 1, 2020

https://dx.doi.org/10.1021/jacs.0c03798
J. Am. Chem. Soc. 2020, 142, 9152–9157

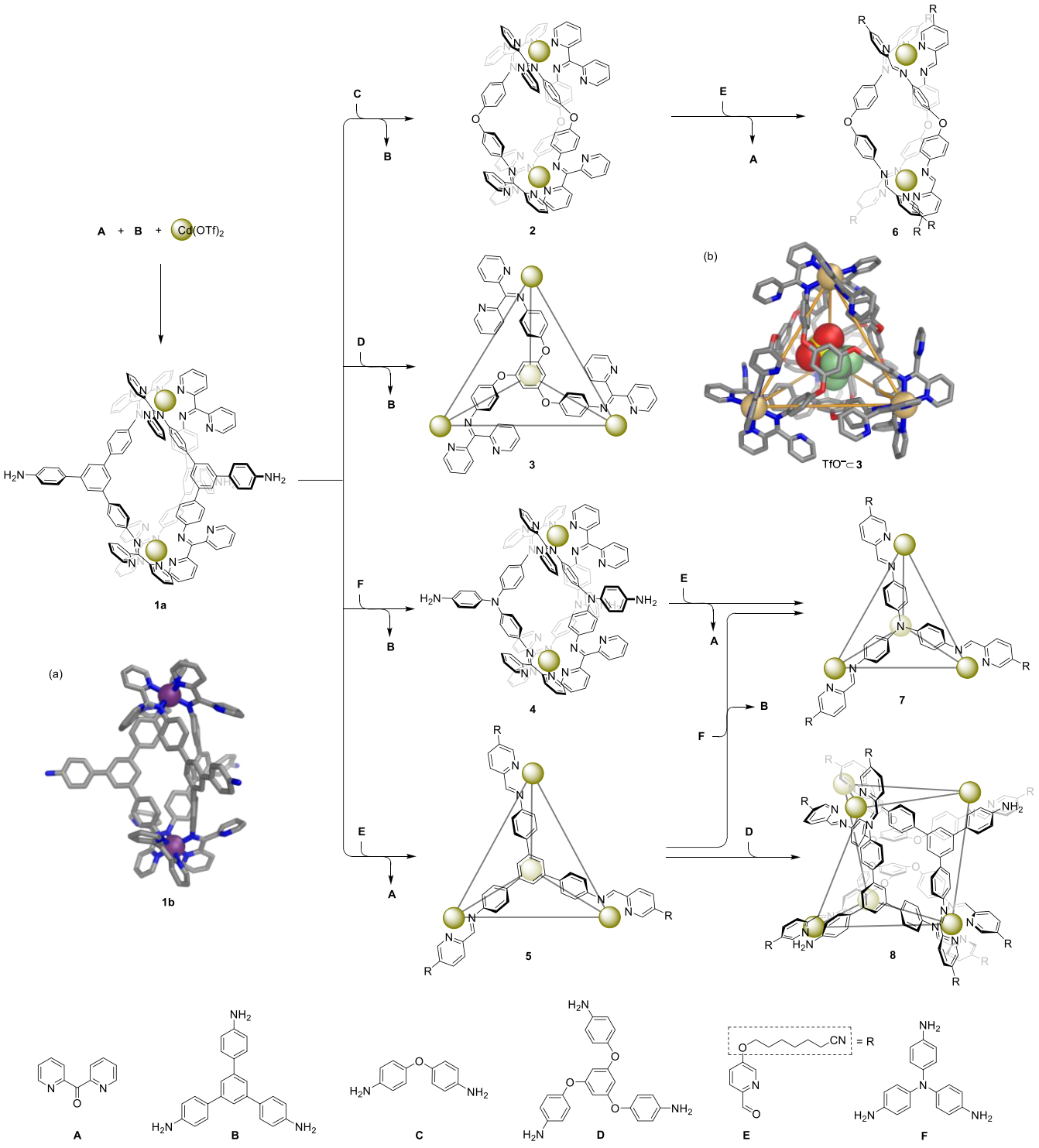

Figure 1. Network of transformations between architectures **1**−**8**, showing the X-ray crystal structures of helicate $Fe^{II}_2L_3$ **1b** (a), which is the Fe^{II} analogue of $Cd^{II}_2L_3$ **1a**, and (b) $TfO^-\subset$**3**. For the crystal structures, disorder, unbound counterions, hydrogen atoms, and solvent of crystallization are omitted for clarity.

S90). As excesses of **C** and **F** were not added, we infer the driving forces for these conversions to have derived from the greater nucleophilicities of the incorporated amines.[16,23]

Analogously, aldehyde **E** (6 equiv) displaced ketone **A** from **2**, resulting in the formation of more stable helicate **6** (Figures S51−S58 and S92). The release of steric encumbrance at the corners after conversion may provide the driving force for this transformation.[18] The incorporation of the long aliphatic chain in subcomponent **E** serves to improve the solubility of the corresponding architectures incorporating **E** (Figure 1), in order to avoid solubility problems during structural transformation.

The addition of more electron-rich triamine **D** (4 equiv) to helicate **1a** (2 equiv) resulted in conversion to tetrahedron **3** along with the release of less electron-rich **B** (6 equiv) (Figures S27−S34 and S89). In addition to the differing nucleophilic-

https://dx.doi.org/10.1021/jacs.0c03798
J. Am. Chem. Soc. 2020, 142, 9152−9157

ities of the amines,[16,23] this transformation may be favored by entropy, as more free particles are present in solution following the substitution reaction. The ^{19}F NMR spectrum of **3** (Figure S29) reveals that a triflate anion resides inside its cavity, indicating that binding of the anion template may provide a further driving force for the transformation.[15d]

The crystal structure of tetrahedron **3** displays approximate *T* point symmetry (Figure 1b). Twelve uncoordinated pyridyl units derived from residues of **A** surround the four vertices of **3**, in similar fashion to the structure of its Zn^{II} analogue.[22] Consistent with the solution-phase ^{19}F NMR spectrum (Figure S29), a triflate anion is encapsulated inside the cavity, occupying 54% of its cavity volume (158 Å^3, Figure S87).

The addition of aldehyde **E** (12 equiv) and additional Cd(OTf)$_2$ (1.33 equiv) to helicate **1a** (1.33 equiv) resulted in its conversion into tetrahedron **5** (Figures S43–S50 and S91). Similarly, the addition of **E** (12 equiv) and Cd(OTf)$_2$ (1.33 equiv) to helicate **4** (1.33 equiv) gave tetrahedron **7** (Figures S59–S66 and S93), releasing subcomponent **A** in both cases. We infer the release of steric hindrance at the corners, as observed in the crystal structure of **1b** (Figure S85), to have driven these transformations.[18] The greater nucleophilicity of triamine subcomponent **F** relative to triamine **B**[16,23] also enabled a tetrahedron-to-tetrahedron transformation from **5** to **7**, following the addition of **F** (4 equiv) to **5** (Figure S94).

The network of transformations shown in Figure 1 culminated in the generation of a new heteroleptic Cd$_6$**L**$_6$**L′**$_2$ twisted trigonal prism **8** (Figures S67–S76), produced following the addition of the more nucleophilic (relative to **B**) subcomponent **D** (2 equiv) to **5** (1.5 equiv) (Figure S95). The composition of the new complex was confirmed by ESI-MS (Figure S75). The homoleptic tetrahedra **5** and **9** were not detected in solution (Figure S95), indicating that integrative self-sorting had occurred to form exclusively the heteroleptic structure.[24] This complex could be also prepared from the three subcomponents **B**, **D**, and **E**, together with cadmium triflate, in a molar ratio of 6:2:18:6. The ^{1}H NMR peaks of **8** (Figures 2a and S67), which displayed the same DOSY diffusion coefficient, are sharp and numerous, consistent with the lower symmetry of the heteroleptic structure.[20]

Slow vapor diffusion of diethyl ether into an acetonitrile solution of **8** provided crystals suitable for X-ray crystallographic analysis. As shown in Figures 2 and S86, Cd$_6$**L**$_6$**L′**$_2$ **8** was revealed to have a twisted trigonal prismatic structure. Six ligands (**L**, formed from imine condensation of **B** with 2 equiv of **E**) define the three twisted rectangular faces, with pairs of these ligands bridging two diagonally opposed cadmium centers with their pyridyl-imine arms. Each equivalent of **B** in **8** contains one unreacted aniline NH$_2$ group, as was also observed for **B** in helicate **1b**. Two ligands (**L′**, formed from imine condensation of **D** with 3 equiv of **E**) define the two triangular faces of the trigonal prism, which are twisted by 35 ± 3° relative to each other. All of the Cd^{II} centers of **8** show facial (fac) coordination and display the same handedness. The framework of **8** thus has approximate D_3 point symmetry. The ^{1}H NMR spectrum of heteroleptic **8** (Figure S67) in solution is consistent with its crystal structure.

The structure of heteroleptic **8** is stabilized by stacking interactions (3.4 Å) between the two central benzene rings of the two triangular faces; it thus lacks an internal cavity. Instead, two bowl-shaped cavities are defined by the two concave **L′** ligands of the triangular faces, with each accommodating a triflate anion (Figure 2b).

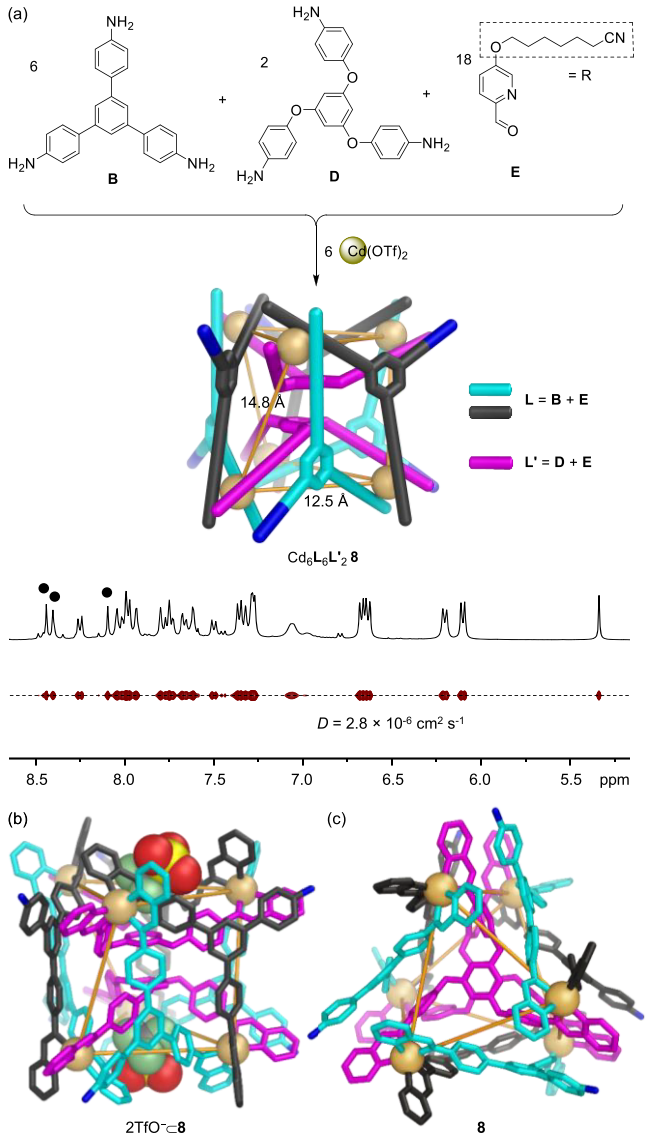

Figure 2. (a) Subcomponent self-assembly of Cd$_6$**L**$_6$**L′**$_2$ **8** and the aromatic region of its ^{1}H DOSY spectrum (400 MHz, 298 K, CD$_3$CN). The three imine peaks of **8** are marked with solid black circles (●). For a full structural assignment, see Figure S67. (b, c) Crystal structure of **8** with (b) and without (c) the two bound triflate anions. Disorder, additional counterions, peripheral R groups on the **E** residues, hydrogen atoms, and solvent of crystallization are omitted for clarity. Only the N atoms of the free amines are colored blue, with the rest of symmetry-equivalent ligands being colored magenta, black, and cyan. Cd^{II} centers are yellow, which are connected by yellow lines to their nearest neighbors. Average Cd^{II}–Cd^{II} distances are labeled in (a).

A series of competition reactions (Figures S96–S102) showed that each of the homoleptic products **2**–**7** (Figure 1) formed selectively in the presence of the subcomponent that was displaced during the formation of that structure in Figure 1, verifying that all transformations resulted in the formation of the thermodynamic product.

The guest binding properties of the helicates listed in Figure 1 were not investigated in solution due to their small internal cavities and large apertures (Figure S85b). Tetrahedron **3** was observed to encapsulate its counteranion, triflate, in slow exchange on the NMR time scale (Figure S29), as noted

https://dx.doi.org/10.1021/jacs.0c03798
J. Am. Chem. Soc. 2020, 142, 9152–9157

above. Neutral molecules, such as cyclohexane, were found to bind within tetrahedron **5** in slow exchange (Figure S103), in similar fashion to the binding behavior observed for its zinc(II) analog.[25] Both tetrahedron **7** and trigonal prism **8** bound AsF_6^- and SbF_6^- in fast exchange on the NMR time scale (Figures S104–S108). Progressive addition of AsF_6^- or SbF_6^- to **8** resulted in clear shifts of the proton signals of the ligands defining the concave triangular faces (Figures S107 and S108), consistent with anions binding in the locations observed in the crystal structure (Figure 2b).

We hypothesized that the selective conversion from one host to another within the transformation network might enable selective guest uptake. To test this idea, we designed a system starting with helicate **1a** and two different guests, triflate and cyclohexane, which are bound by tetrahedra **3** and **5**, respectively. As shown in Figure 3, after addition of

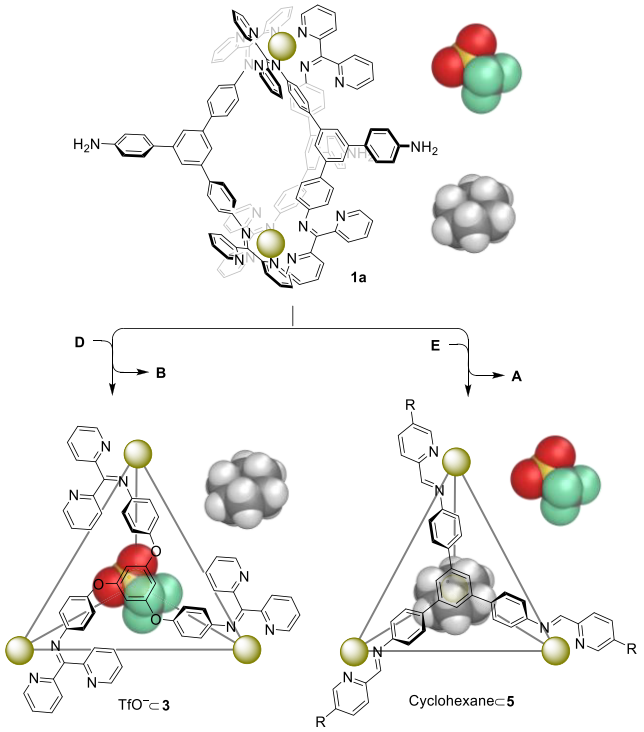

Figure 3. Schematic representation of selective uptake of either triflate or cyclohexane upon structural transformations.

subcomponent **D** to the system, helicate **1a** converted into **3**, which took up the triflate guest selectively from solution (Figure S109). In contrast, the addition of **E** to **1a** resulted in displacement of the ketone subcomponents, producing **5** and selectively binding cyclohexane (Figure S110).

Subcomponent displacement thus offers a versatile strategy for structural transformations between different complex assemblies, allowing selective guest uptake following structural transformation. A new type of $M_6L_6L'_2$ twisted trigonal prism was produced using this strategy, the guest binding properties of which are of interest.[20] Studies to expand the generality of its formation with other tritopic or ditopic ligands and to achieve heteroleptic architectures with new guest binding properties are currently underway.

■ ASSOCIATED CONTENT

Supporting Information

The Supporting Information is available free of charge at https://pubs.acs.org/doi/10.1021/jacs.0c03798.

Complete experimental details (PDF)
X-ray data for **1b** (CCDC 1987033) (CIF)
X-ray data for **3** (CCDC 1987032) (CIF)
X-ray data for **8** (CCDC 1987034) (CIF)

■ AUTHOR INFORMATION

Corresponding Authors

Lin Xu − *Department of Chemistry, University of Cambridge, Cambridge CB2 1EW, United Kingdom; Shanghai Key Laboratory of Green Chemistry and Chemical Processes, School of Chemistry and Molecular Engineering, East China Normal University, Shanghai 200062, P. R. China*; Email: lxu@chem.ecnu.edu.cn

Jonathan R. Nitschke − *Department of Chemistry, University of Cambridge, Cambridge CB2 1EW, United Kingdom*; orcid.org/0000-0002-4060-5122; Email: jrn34@cam.ac.uk

Authors

Dawei Zhang − *Department of Chemistry, University of Cambridge, Cambridge CB2 1EW, United Kingdom*; orcid.org/0000-0002-0898-9795

Tanya K. Ronson − *Department of Chemistry, University of Cambridge, Cambridge CB2 1EW, United Kingdom*; orcid.org/0000-0002-6917-3685

Complete contact information is available at: https://pubs.acs.org/10.1021/jacs.0c03798

Notes

The authors declare no competing financial interest.

■ ACKNOWLEDGMENTS

This work was supported by the European Research Council (695009) and the UK Engineering and Physical Sciences Research Council (EPSRC EP/P027067/1). The authors thank the Department of Chemistry NMR facility, University of Cambridge for performing some NMR experiments, the EPSRC UK National Mass Spectrometry Facility at Swansea University for carrying out high resolution mass spectrometry and Diamond Light Source (UK) for synchrotron beamtime on I19 (MT11397). L.X. acknowledges the National Nature Science Foundation of China (Nos. 21922506, 21672070, and 21871092) and Shanghai Pujiang Program (No. 18PJD015). D.Z. acknowledges a Herchel Smith Research Fellowship from the University of Cambridge.

■ REFERENCES

(1) (a) Wang, W.; Wang, Y. X.; Yang, H. B. Supramolecular transformations within discrete coordination-driven supramolecular architectures. *Chem. Soc. Rev.* **2016**, *45*, 2656–2693. (b) Zhou, X. P.; Wu, Y.; Li, D. Polyhedral metal-imidazolate cages: control of self-assembly and cage to cage transformation. *J. Am. Chem. Soc.* **2013**, *135*, 16062–16065.

(2) (a) Saibil, H. R.; Fenton, W. A.; Clare, D. K.; Horwich, A. L. Structure and allostery of the chaperonin GroEL. *J. Mol. Biol.* **2013**, *425*, 1476–1487. (b) Nussinov, R. Introduction to protein ensembles and allostery. *Chem. Rev.* **2016**, *116*, 6263–6266.

(3) (a) Carlier, P. R. Threading the needle: mimicking natural toroidal catalysts. *Angew. Chem., Int. Ed.* **2004**, *43*, 2602–2605.

(b) Raynal, M.; Ballester, P.; Vidal-Ferran, A.; van Leeuwen, P. W. Supramolecular catalysis. Part 2: artificial enzyme mimics. *Chem. Soc. Rev.* **2014**, *43*, 1734−1787. (c) Hong, C. M.; Bergman, R. G.; Raymond, K. N.; Toste, F. D. Self-assembled tetrahedral hosts as supramolecular catalysts. *Acc. Chem. Res.* **2018**, *51*, 2447−2455. (d) Zhang, Q.; Tiefenbacher, K. Terpene cyclization catalysed inside a self-assembled cavity. *Nat. Chem.* **2015**, *7*, 197−202. (e) Galli, M.; Lewis, J. E.; Goldup, S. M. A stimuli-responsive rotaxane-gold catalyst: regulation of activity and diastereoselectivity. *Angew. Chem., Int. Ed.* **2015**, *54*, 13545−13549. (f) Eichstaedt, K.; Jaramillo-Garcia, J.; Leigh, D. A.; Marcos, V.; Pisano, S.; Singleton, T. A. Switching between anion-binding catalysis and aminocatalysis with a rotaxane dual-function catalyst. *J. Am. Chem. Soc.* **2017**, *139*, 9376−9381.

(4) (a) Choi, S.; Mukhopadhyay, R. D.; Kim, Y.; Hwang, I. C.; Hwang, W.; Ghosh, S. K.; Baek, K.; Kim, K. Fuel-driven transient crystallization of a cucurbit[8]uril-based host-guest complex. *Angew. Chem., Int. Ed.* **2019**, *58*, 16850−16853. (b) Kang, S. I.; Lee, M.; Lee, D. Weak links to differentiate weak bonds: size-selective response of π-conjugated macrocycle gels to ammonium ions. *J. Am. Chem. Soc.* **2019**, *141*, 5980−5986. (c) Hasell, T.; Cooper, A. I. Porous organic cages: soluble, modular and molecular pores. *Nat. Rev. Mater.* **2016**, *1*, 16053. (d) Frischmann, P. D.; MacLachlan, M. J. Metallocavitands: an emerging class of functional multimetallic host molecules. *Chem. Soc. Rev.* **2013**, *42*, 871−890. (e) Yang, H.; Yuan, B.; Zhang, X.; Scherman, O. A. Supramolecular chemistry at interfaces: host-guest interactions for fabricating multifunctional biointerfaces. *Acc. Chem. Res.* **2014**, *47*, 2106−2115. (f) Custelcean, R. Anion encapsulation and dynamics in self-assembled coordination cages. *Chem. Soc. Rev.* **2014**, *43*, 1813−1824. (g) Foianesi-Takeshige, L. H.; Takahashi, S.; Tateishi, T.; Sekine, R.; Okazawa, A.; Zhu, W.; Kojima, T.; Harano, K.; Nakamura, E.; Sato, H.; Hiraoka, S. Bifurcation of self-assembly pathways to sheet or cage controlled by kinetic template effect. *Commun. Chem.* **2019**, *2*, 128. (h) Wang, S.; Sawada, T.; Ohara, K.; Yamaguchi, K.; Fujita, M. Capsule-capsule conversion by guest encapsulation. *Angew. Chem., Int. Ed.* **2016**, *55*, 2063−2066. (i) Zhiquan, L.; Xie, H.; Border, S. E.; Gallucci, J.; Pavlovic, R. Z.; Badjic, J. D. A stimuli-responsive molecular capsule with switchable dynamics, chirality, and encapsulation characteristics. *J. Am. Chem. Soc.* **2018**, *140*, 11091−11100. (j) Liu, Y.; Zhao, W.; Chen, C. H.; Flood, A. H. Chloride capture using a C-H hydrogen-bonding cage. *Science* **2019**, *365*, 159−161.

(5) (a) Kishi, N.; Akita, M.; Kamiya, M.; Hayashi, S.; Hsu, H. F.; Yoshizawa, M. Facile catch and release of fullerenes using a photoresponsive molecular tube. *J. Am. Chem. Soc.* **2013**, *135*, 12976−12979. (b) Dube, H.; Ajami, D.; Rebek, J., Jr. Photochemical control of reversible encapsulation. *Angew. Chem., Int. Ed.* **2010**, *49*, 3192−3195. (c) Han, M.; Michel, R.; He, B.; Chen, Y. S.; Stalke, D.; John, M.; Clever, G. H. Light-triggered guest uptake and release by a photochromic coordination cage. *Angew. Chem., Int. Ed.* **2013**, *52*, 1319−1323. (d) Kim, T. Y.; Vasdev, R. A. S.; Preston, D.; Crowley, J. D. Strategies for reversible guest uptake and release from metallosupramolecular architectures. *Chem. - Eur. J.* **2018**, *24*, 14878−14890. (e) Samanta, S. K.; Quigley, J.; Vinciguerra, B.; Briken, V.; Isaacs, L. Cucurbit[7]uril enables multi-stimuli-responsive release from the self-assembled hydrophobic phase of a metal organic polyhedron. *J. Am. Chem. Soc.* **2017**, *139*, 9066−9074. (f) Wu, H.; Chen, Y.; Zhang, L.; Anamimoghadam, O.; Shen, D.; Liu, Z.; Cai, K.; Pezzato, C.; Stern, C. L.; Liu, Y.; Stoddart, J. F. A dynamic tetracationic macrocycle exhibiting photoswitchable molecular encapsulation. *J. Am. Chem. Soc.* **2019**, *141*, 1280−1289.

(6) Chen, J.; Wezenberg, S. J.; Feringa, B. L. Intramolecular transport of small-molecule cargo in a nanoscale device operated by light. *Chem. Commun.* **2016**, *52*, 6765−6768.

(7) Shanmugaraju, S.; Umadevi, D.; Savyasachi, A. J.; Byrne, K.; Ruether, M.; Schmitt, W.; Watson, G. W.; Gunnlaugsson, T. Reversible adsorption and storage of secondary explosives from water using a Tröger's base-functionalised polymer. *J. Mater. Chem. A* **2017**, *5*, 25014−25024.

(8) (a) Cullen, W.; Turega, S.; Hunter, C. A.; Ward, M. D. pH-dependent binding of guests in the cavity of a polyhedral coordination cage: reversible uptake and release of drug molecules. *Chem. Sci.* **2015**, *6*, 625−631. (b) Mura, S.; Nicolas, J.; Couvreur, P. Stimuli-responsive nanocarriers for drug delivery. *Nat. Mater.* **2013**, *12*, 991−1003. (c) Giglio, V.; Varela-Aramburu, S.; Travaglini, L.; Fiorini, F.; Seeberger, P. H.; Maggini, L.; De Cola, L. Reshaping silica particles: mesoporous nanodiscs for bimodal delivery and improved cellular uptake. *Chem. Eng. J.* **2018**, *340*, 148−154.

(9) (a) Chen, S.; Chen, L. J.; Yang, H. B.; Tian, H.; Zhu, W. Light-triggered reversible supramolecular transformations of multi-bisthienylethene hexagons. *J. Am. Chem. Soc.* **2012**, *134*, 13596−13599. (b) Oldknow, S.; Martir, D. R.; Pritchard, V. E.; Blitz, M. A.; Fishwick, C. W. G.; Zysman-Colman, E.; Hardie, M. J. Structure-switching M_3L_2 Ir(III) coordination cages with photo-isomerising azo-aromatic linkers. *Chem. Sci.* **2018**, *9*, 8150−8159. (c) Diaz-Moscoso, A.; Ballester, P. Light-responsive molecular containers. *Chem. Commun.* **2017**, *53*, 4635−4652.

(10) (a) Kishimoto, M.; Kondo, K.; Akita, M.; Yoshizawa, M. A pH-responsive molecular capsule with an acridine shell: catch and release of large hydrophobic compounds. *Chem. Commun.* **2017**, *53*, 1425−1428. (b) Kim, S. H.; Kim, K. R.; Ahn, D. R.; Lee, J. E.; Yang, E. G.; Kim, S. Y. Reversible regulation of enzyme activity by pH-responsive encapsulation in DNA nanocages. *ACS Nano* **2017**, *11*, 9352−9359. (c) Kaizerman-Kane, D.; Hadar, M.; Tal, N.; Dobrovetsky, R.; Zafrani, Y.; Cohen, Y. pH-responsive pillar[6]arene-based water-soluble supramolecular hexagonal boxes. *Angew. Chem., Int. Ed.* **2019**, *58*, 5302−5306.

(11) (a) Wang, S.; Yao, C.; Ni, M.; Xu, Z.; Cheng, M.; Hu, X.-Y.; Shen, Y.-Z.; Lin, C.; Wang, L.; Jia, D. Thermo- and oxidation-responsive supramolecular vesicles constructed from self-assembled pillar[6]arene-ferrocene based amphiphilic supramolecular diblock copolymers. *Polym. Chem.* **2017**, *8*, 682−688. (b) Zhang, D.; Ronson, T. K.; Guryel, S.; Thoburn, J. D.; Wales, D. J.; Nitschke, J. R. Temperature controls guest uptake and release from Zn_4L_4 tetrahedra. *J. Am. Chem. Soc.* **2019**, *141*, 14534−14538. (c) Chan, M. H.; Leung, S. Y.; Yam, V. W. Rational design of multi-stimuli-responsive scaffolds: synthesis of luminescent oligo(ethynylpyridine)-containing alkynylplatinum(II) polypyridine foldamers stabilized by Pt···Pt interactions. *J. Am. Chem. Soc.* **2019**, *141*, 12312−12321.

(12) (a) Heo, J.; Jeon, Y. M.; Mirkin, C. A. Reversible interconversion of homochiral triangular macrocycles and helical coordination polymers. *J. Am. Chem. Soc.* **2007**, *129*, 7712−7713. (b) Baxter, P. N. W.; Khoury, R. G.; Lehn, J.-M.; Baum, G.; Fenske, D. Adaptive self-assembly: environment-induced formation and reversible switching of polynuclear metallocyclophanes. *Chem. - Eur. J.* **2000**, *6*, 4140−4148. (c) Kilbas, B.; Mirtschin, S.; Scopelliti, R.; Severin, K. A solvent-responsive coordination cage. *Chem. Sci.* **2012**, *3*, 701−704. (d) Gidron, O.; Jirasek, M.; Trapp, N.; Ebert, M. O.; Zhang, X.; Diederich, F. Homochiral [2]catenane and bis[2]catenane from alleno-acetylenic helicates - a highly selective narcissistic self-sorting process. *J. Am. Chem. Soc.* **2015**, *137*, 12502−12505. (e) Zhang, Z.; Kim, D. S.; Lin, C. Y.; Zhang, H.; Lammer, A. D.; Lynch, V. M.; Popov, I.; Miljanic, O. S.; Anslyn, E. V.; Sessler, J. L. Expanded porphyrin-anion supramolecular assemblies: environmentally responsive sensors for organic solvents and anions. *J. Am. Chem. Soc.* **2015**, *137*, 7769−7774.

(13) (a) Frischmann, P. D.; Kunz, V.; Stepanenko, V.; Wurthner, F. Subcomponent self-assembly of a 4 nm M_4L_6 tetrahedron with Zn(II) vertices and perylene bisimide dye edges. *Chem. - Eur. J.* **2015**, *21*, 2766−2769. (b) Weilandt, T.; Troff, R. W.; Saxell, H.; Rissanen, K.; Schalley, C. A. Metallo-supramolecular self-assembly: the case of triangle-square equilibria. *Inorg. Chem.* **2008**, *47*, 7588−7598. (c) Lu, X.; Li, X.; Guo, K.; Xie, T. Z.; Moorefield, C. N.; Wesdemiotis, C.; Newkome, G. R. Probing a hidden world of molecular self-assembly: concentration-dependent, three-dimensional supramolecular interconversions. *J. Am. Chem. Soc.* **2014**, *136*, 18149−18155. (d) Yamamoto, T.; Arif, A. M.; Stang, P. J. Dynamic equilibrium of a supramolecular dimeric rhomboid and trimeric hexagon and determination of its

https://dx.doi.org/10.1021/jacs.0c03798
J. Am. Chem. Soc. 2020, 142, 9152−9157

thermodynamic constants. *J. Am. Chem. Soc.* **2003**, *125*, 12309−12317.
(14) (a) Ozores, H. L.; Amorin, M.; Granja, J. R. Self-assembling molecular capsules based on α,γ-cyclic peptides. *J. Am. Chem. Soc.* **2017**, *139*, 776−784. (b) Zhou, J.; Zhang, Y.; Yu, G.; Crawley, M. R.; Fulong, C. R. P.; Friedman, A. E.; Sengupta, S.; Sun, J.; Li, Q.; Huang, F.; Cook, T. R. Highly emissive self-assembled BODIPY-platinum supramolecular triangles. *J. Am. Chem. Soc.* **2018**, *140*, 7730−7736. (c) Akine, S.; Miyashita, M.; Nabeshima, T. A metallo-molecular cage that can close the apertures with coordination bonds. *J. Am. Chem. Soc.* **2017**, *139*, 4631−4634. (d) Burke, B. P.; Grantham, W.; Burke, M. J.; Nichol, G. S.; Roberts, D.; Renard, I.; Hargreaves, R.; Cawthorne, C.; Archibald, S. J.; Lusby, P. J. Visualizing kinetically robust $Co^{III}_4L_6$ assemblies in vivo: SPECT imaging of the encapsulated $[^{99m}Tc]TcO_4^-$ anion. *J. Am. Chem. Soc.* **2018**, *140*, 16877−16881. (e) Bhat, I. A.; Samanta, D.; Mukherjee, P. S. A Pd_{24} pregnant molecular nanoball: self-templated stellation by precise mapping of coordination sites. *J. Am. Chem. Soc.* **2015**, *137*, 9497−9502. (f) Pramanik, S.; Aprahamian, I. Hydrazone switch-based negative feedback loop. *J. Am. Chem. Soc.* **2016**, *138*, 15142−15145. (g) Ward, M. D.; Hunter, C. A.; Williams, N. H. Coordination cages based on bis(pyrazolylpyridine) ligands: structures, dynamic behavior, guest binding, and catalysis. *Acc. Chem. Res.* **2018**, *51*, 2073−2082. (h) Li, K.; Zhang, L. Y.; Yan, C.; Wei, S. C.; Pan, M.; Zhang, L.; Su, C. Y. Stepwise assembly of $Pd_6(RuL_3)_8$ nanoscale rhombododecahedral metal-organic cages via metalloligand strategy for guest trapping and protection. *J. Am. Chem. Soc.* **2014**, *136*, 4456−4459.
(15) (a) Zhang, D.; Ronson, T. K.; Nitschke, J. R. Functional capsules via subcomponent self-assembly. *Acc. Chem. Res.* **2018**, *51*, 2423−2436. (b) Yi, S.; Brega, V.; Captain, B.; Kaifer, A. E. Sulfate-templated self-assembly of new M_4L_6 tetrahedral metal organic cages. *Chem. Commun.* **2012**, *48*, 10295−10297. (c) Yang, L.; Jing, X.; He, C.; Chang, Z.; Duan, C. Redox-active M_8L_6 cubic hosts with tetraphenylethylene faces encapsulate organic dyes for light-driven H_2 production. *Chem. - Eur. J.* **2016**, *22*, 18107−18114. (d) Ferguson, A.; Staniland, R. W.; Fitchett, C. M.; Squire, M. A.; Williamson, B. E.; Kruger, P. E. Variation of guest selectivity within $[Fe_4L_4]^{8+}$ tetrahedral cages through subtle modification of the face-capping ligand. *Dalton Trans.* **2014**, *43*, 14550−14553.
(16) Nitschke, J. R. Construction, substitution, and sorting of metallo-organic structures via subcomponent self-assembly. *Acc. Chem. Res.* **2007**, *40*, 103−112.
(17) (a) Ren, D. H.; Qiu, D.; Pang, C. Y.; Li, Z.; Gu, Z. G. Chiral tetrahedral iron(II) cages: diastereoselective subcomponent self-assembly, structure interconversion and spin-crossover properties. *Chem. Commun.* **2015**, *51*, 788−791. (b) Wiley, C. A.; Holloway, L. R.; Miller, T. F.; Lyon, Y.; Julian, R. R.; Hooley, R. J. Electronic effects on narcissistic self-sorting in multicomponent self-assembly of Fe-iminopyridine meso-helicates. *Inorg. Chem.* **2016**, *55*, 9805−9815. (c) Meng, W.; Ronson, T. K.; Clegg, J. K.; Nitschke, J. R. Transformations within a network of cadmium architectures. *Angew. Chem., Int. Ed.* **2013**, *52*, 1017−1021.
(18) (a) Hardy, M.; Struch, N.; Holstein, J. J.; Schnakenburg, G.; Wagner, N.; Engeser, M.; Beck, J.; Clever, G. H.; Lutzen, A. Dynamic complex-to-complex transformations of heterobimetallic systems influence the cage structure or spin state of iron(II)ions. *Angew. Chem., Int. Ed.* **2020**, *59*, 3195−3200. (b) McConnell, A. J.; Aitchison, C. M.; Grommet, A. B.; Nitschke, J. R. Subcomponent exchange transforms an $Fe^{II}_4L_4$ cage from high- to low-spin, switching guest release in a two-cage system. *J. Am. Chem. Soc.* **2017**, *139*, 6294−6297.
(19) Rizzuto, F. J.; Carpenter, J. P.; Nitschke, J. R. Multisite binding of drugs and natural products in an entropically favorable, heteroleptic receptor. *J. Am. Chem. Soc.* **2019**, *141*, 9087−9095.
(20) (a) De, S.; Mahata, K.; Schmittel, M. Metal-coordination-driven dynamic heteroleptic architectures. *Chem. Soc. Rev.* **2010**, *39*, 1555−1575. (b) Pullen, S.; Clever, G. H. Mixed-ligand metal-organic frameworks and heteroleptic coordination cages as multifunctional scaffolds-a comparison. *Acc. Chem. Res.* **2018**, *51*, 3052−3064. (c) Bardhan, D.; Chand, D. K. Palladium(II)-based self-assembled heteroleptic coordination architectures: a growing family. *Chem. - Eur. J.* **2019**, *25*, 12241−12269.
(21) (a) Sokkalingam, P.; Shraberg, J.; Rick, S. W.; Gibb, B. C. Binding hydrated anions with hydrophobic pockets. *J. Am. Chem. Soc.* **2016**, *138*, 48−51. (b) Busschaert, N.; Caltagirone, C.; Van Rossom, W.; Gale, P. A. Applications of supramolecular anion recognition. *Chem. Rev.* **2015**, *115*, 8038−8155. (c) Langton, M. J.; Serpell, C. J.; Beer, P. D. Anion recognition in water: recent advances from a supramolecular and macromolecular perspective. *Angew. Chem., Int. Ed.* **2016**, *55*, 4629−4629. (d) Kang, S. O.; Llinares, J. M.; Day, V. W.; Bowman-James, K. Cryptand-like anion receptors. *Chem. Soc. Rev.* **2010**, *39*, 3980−4003. (e) Kubik, S. Anion recognition in water. *Chem. Soc. Rev.* **2010**, *39*, 3648−3663. (f) Lisbjerg, M.; Valkenier, H.; Jessen, B. M.; Al-Kerdi, H.; Davis, A. P.; Pittelkow, M. Biotin[6]uril esters: chloride-selective transmembrane anion carriers employing C-H···anion interactions. *J. Am. Chem. Soc.* **2015**, *137*, 4948−4951. (g) Shyshov, O.; Siewerth, K. A.; von Delius, M. Evidence for anion-binding of all-cis hexafluorocyclohexane in solution and solid state. *Chem. Commun.* **2018**, *54*, 4353−4355. (h) Deng, C. L.; Bard, J. P.; Lohrman, J. A.; Barker, J. E.; Zakharov, L. N.; Johnson, D. W.; Haley, M. M. Exploiting the hydrogen bond donor/acceptor properties of PN-heterocycles: selective anion receptors for hydrogen sulfate. *Angew. Chem., Int. Ed.* **2019**, *58*, 3934−3938.
(22) Xu, L.; Zhang, D.; Ronson, T.; Nitschke, J. Improved acid resistance of a metal-organic cage enables cargo release and exchange between hosts. *Angew. Chem., Int. Ed.* **2020**, *59*, 7435.
(23) (a) Ayme, J.-F.; Lehn, J.-M. Self-sorting of two imine-based metal complexes: balancing kinetics and thermodynamics in constitutional dynamic networks. *Chem. Sci.* **2020**, *11*, 1114−1121. (b) Belowich, M. E.; Stoddart, J. F. Dynamic imine chemistry. *Chem. Soc. Rev.* **2012**, *41*, 2003−2024.
(24) (a) He, Z.; Jiang, W.; Schalley, C. A. Integrative self-sorting: a versatile strategy for the construction of complex supramolecular architecture. *Chem. Soc. Rev.* **2015**, *44*, 779−789. (b) Beaudoin, D.; Rominger, F.; Mastalerz, M. Chiral self-sorting of [2 + 3] salicylimine cage compounds. *Angew. Chem., Int. Ed.* **2017**, *56*, 1244−1248. (c) Wang, Y. S.; Feng, T.; Wang, Y. Y.; Hahn, F. E.; Han, Y. F. Homo- and heteroligand poly-NHC metal assemblies: synthesis by narcissistic and social self-sorting. *Angew. Chem., Int. Ed.* **2018**, *57*, 15767−15771.
(25) Castilla, A. M.; Ronson, T. K.; Nitschke, J. R. Sequence-dependent guest release triggered by orthogonal chemical signals. *J. Am. Chem. Soc.* **2016**, *138*, 2342−2351.

https://dx.doi.org/10.1021/jacs.0c03798
J. Am. Chem. Soc. 2020, 142, 9152−9157